Available online at www.sciencedirect.com
SCIENCE DIRECT®
Nuclear Instruments and Methods in Physics Research A 513 (2003) 639–643
NUCLEAR INSTRUMENTS & METHODS IN PHYSICS RESEARCH Section A
www.elsevier.com/locate/nima

X-ray polarimetry with an active-matrix pixel proportional counter

J.K. Black[a,*], P. Deines-Jones[b], S.E. Ready[c], R.A. Street[c]

[a] Forbin Scientific, Code 662, NASA/Goddard Space Flight Center, Greenbelt, MD 20771, USA
[b] Universities Space Research Association, Code 662, NASA/Goddard Space Flight Center, Greenbelt, MD 20771, USA
[c] Palo Alto Research Center, 3333 Coyote Hill Road, Palo Alto, CA 94304, USA

Received 1 April 2003; accepted 7 July 2003

Abstract

We report the first results from an X-ray polarimeter with a micropattern gas proportional counter using an amorphous silicon active matrix readout. With 100% polarized X-rays at 4.5 keV, we obtain a modulation factor of 0.33 ± 0.03, confirming previous reports of the high polarization sensitivity of a finely segmented pixel proportional counter. The detector described here has a geometry suitable for the focal plane of an astronomical X-ray telescope. Amorphous silicon readout technology will enable additional extensions and improvements.

PACS: 07.60.Fs; 07.85.Fv; 29.40.Gx; 95.55.Ka

Keywords: X-ray polarimetry; Particle tracking; Proportional counter; GEM; Pixel readout

The prospects for X-ray polarimetry as a practical tool have been revolutionized by the recent introduction of an instrument with unprecedented sensitivity [1–3]. Based on the photoelectric effect, this new type of polarimeter uses a finely spaced, gas pixel detector to image the tracks of photoelectrons. Polarization information is obtained by determining the angle of emission of the photoelectron, which is correlated with the electric field vector of the X-ray.

The primary innovation of this new polarimeter is the introduction of a pixel readout anode to a micro-pattern gas proportional counter. With a pixel size small compared to the photoelectron range, photoelectron tracks can be imaged and the emission angle reconstructed event-by-event. Combined with the high quantum efficiency and broad bandpass of the photoelectric effect, this non-dispersive technique gives dramatic improvements in sensitivity over polarimeters based on X-ray scattering [4].

Further improvements in the pixel anode will allow this new polarimetry technique to realize its full potential. The polarimeters demonstrated previously consist of a gas electron multiplier (GEM) [5] suspended above a readout plane segmented into individual pixels. Each pixel is connected to a chain of readout electronics through a multi-layer fine-line printed circuit. This type of pixel anode limits both the pixel spacing

*Corresponding author. Tel.: +1-301-286-1231; fax: +1-301-286-1684.
E-mail address: black@forbinsci.com (J.K. Black).

0168-9002/$ - see front matter
doi:10.1016/j.nima.2003.07.015

and the total number of pixels. An anode plane with integrated active electronics, such as CMOS VLSI [3], would overcome this limitation.

Another possible active pixel anode plane is an amorphous silicon thin-film transistor (TFT) array like those used in flat-panel imagers [6]. In this active-matrix-addressing scheme, each pixel is connected to readout electronics through a TFT that acts as an analog switch. Charge is held on the pixel until the transistor is activated, allowing a multiplexed readout such that n^2 pixels are read out with $2n$ electronic channels.

We report the first results from a polarimeter with TFT active-matrix readout and a geometric area suitable for the focal plane of a typical X-ray astronomical telescope with conical foil mirrors [7,8]. We recorded photoelectron track images from 5.9 and 20 keV X-rays and made polarization measurements at 4.5 keV.

The detector, shown schematically in Fig. 1, consisted of a double-GEM with 100-μm hexagonal pitch and a TFT pixel anode with 100-μm square pitch. The active area was defined by the double-GEM, which was 12 mm × 12 mm. Only a small fraction of the TFT array's 512 × 512 pixels

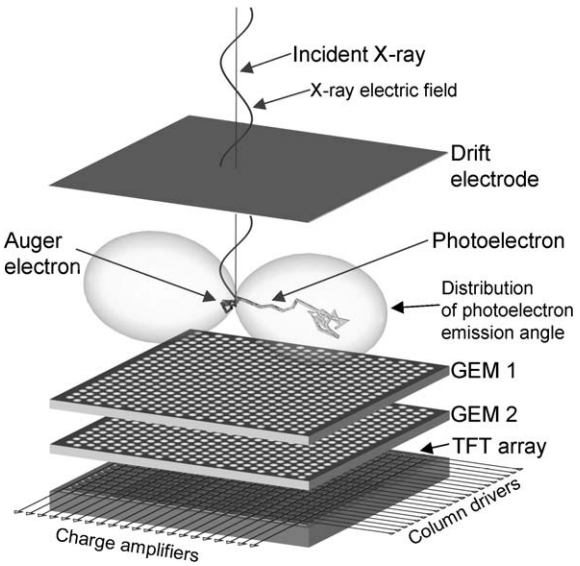

Fig. 1. Schematic diagram of detector geometry used in these measurements. The $\sin^2\theta\cos^2\phi$ distribution of photoelectron emission for normally incident X-rays is projected onto the detector plane and observed as $\cos^2\phi$.

(about 25 cm^2) was used. No attempt was made to align the GEMs with each other or with the TFT array.

The GEMs were contained in a detector body with a thin polyimide entrance window. The active depth was 3 mm, determined by the spacing between a nickel mesh drift electrode and the GEMs. The spacing between GEMs was 750 μm. The spacing between the GEMs and the TFT array was maintained by a 750 μm thick silicone gasket that also acted as a gas seal. The detector was operated as a flow counter using an 80% neon, 20% CO_2 gas mixture at an apparent gain of about 10^4. The drift field was 300 V/cm.

We fabricated the GEMs by UV laser ablation [9,10] in the Laboratory for High Energy Astrophysics at NASA's Goddard Space Flight Center (GSFC). The GEMs were 75 μm thick with hole diameters that were 60 μm at the electrodes, constricting to 50 μm in the center of the substrate.

The TFT pixel arrays were fabricated at the Palo Alto Research Center using a process scalable to large areas ($\sim 10^3$ cm^2). Each pixel contains a metal anode pad, a storage capacitor of about 0.4 pF and a TFT switch. The pixel design is described in more detail elsewhere [11,12]. The source of the TFT is connected to the anode pad, which is isolated from the rest of the pixel by an insulation layer. The anode pads cover about 67% of the surface area. The TFT gates are connected in columns and the drains are connected in rows.

With the TFT switches open, charge from the GEMs is stored on the anode pads. To read out the array, the TFT switches are closed column-by-column by activating the gates lines, so that charge is transferred from a column of anode pads to a row of external amplifiers [6]. Typical operating conditions turn on the TFT gate for 20–30 μs, which is nearly 10 times the RC time constant of the TFT resistance and pixel capacitance. The signal is digitized to 14 bits using correlated double sampling. Electronic noise is less than 1000 electrons (rms). For these measurements, the array was operated in a scanning mode at a frequency of 6 Hz.

Fig. 2 shows a sample of tracks recorded from 5.9 keV X-rays. Most of the charge is deposited at the end of the photoelectron track. At the

beginning of the track is a smaller cluster of charge deposited by the Auger electron (870 eV in neon), which is emitted isotropically.

Significantly more structure is seen in tracks from 20 keV photons as shown in Fig. 3. The Auger/interaction point can still be identified among more hard scatters and knock-on electrons. These tracks emphasize that large-area detectors of this type could be used to track high-energy electrons or minimum ionizing particles.

At 4.5 keV, most of this fine structure is obscured by the diffusion of the primary electrons in the drift volume as shown in Fig. 3. Nevertheless, the track images have a discernable direction.

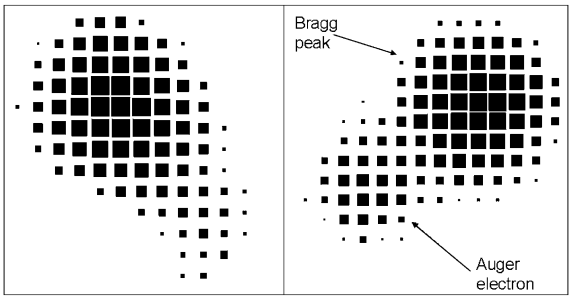

Fig. 2. Example track images from 5.9 keV X-rays. The boxes are on a 100 μm grid. The area of each box represents the total charge collected in the pixel. Two peaks are visible in the distribution. The smaller peak is due to the Auger electron, emitted at the X-ray interaction point.

We produced polarized photons by reflecting X-rays at 90° off a silicon crystal. The X-rays were produced by a tube with a titanium anode ($K_\alpha = 4.5$ keV). The X-ray tube and crystal were mounted on a swivel arm that allowed the plane of polarization to be rotated with respect to the detector coordinate system as shown in Fig. 4. Data were collected with the plane of X-ray polarization (ϕ_{pol}) at three different angles, separated by about 45°.

We analyzed the polarized data first by reconstructing the emission angle of each photoelectron. We then fit histograms of the emission angles to the expected functional form: $N(\phi) = A + B\cos^2(\phi - \phi_{\mathrm{pol}})$, where ϕ_{pol} is the angle of the plane of polarization. The sensitivity to polarization is defined by the modulation μ:

$$\mu = (N_{\max} - N_{\min})/(N_{\max} + N_{min}) = B/(2A + B)$$

where $N_{\max}$ and $N_{\min}$ are the maximum and minimum of the function, respectively.

We estimated the direction of photoelectron emission of each event as the direction of the major axis of the second moment of the charge distribution. Specifically, we calculated the angle of emission as the angle ϕ that minimized the second moment M of the total charge distribution

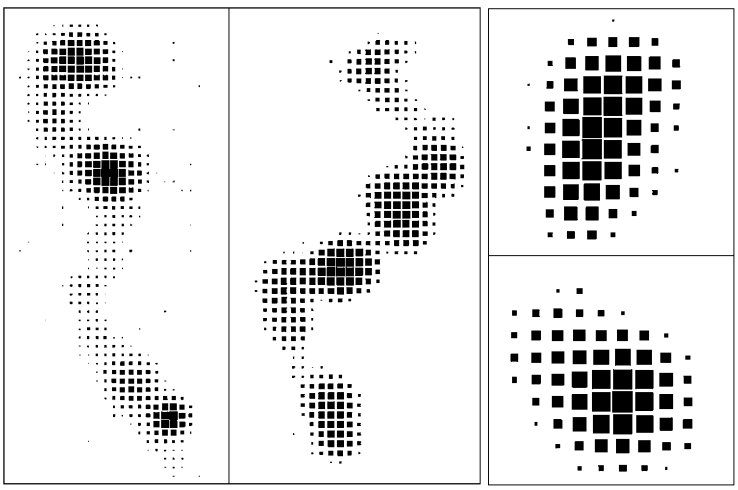

Fig. 3. Track images from 20 keV X-rays (left) and 4.5 keV X-rays (right).

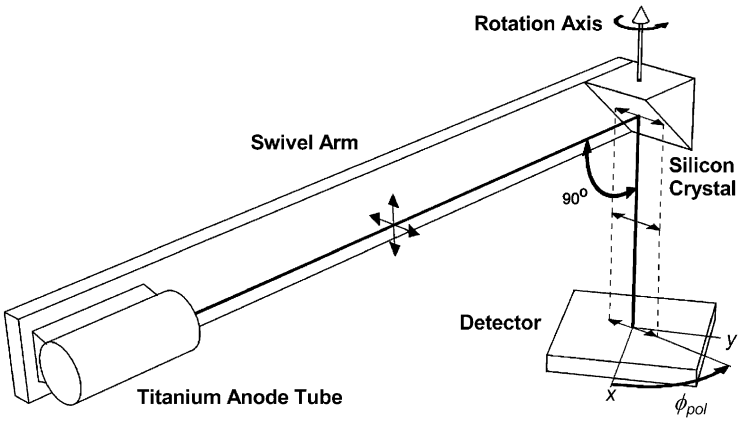

Fig. 4. Experimental setup for polarization measurements. Polarized X-rays at 4.5 keV were produced by scattering at 90° off a silicon crystal mounted above the detector. The tube and crystal were mounted on a swiveled arm that allowed the plane of polarization to be rotated with respect to the detector coordinate system by the angle $\phi_{\rm pol}$.

with barycenter coordinates $(x_{\rm b}, y_{\rm b})$:

$$M = \frac{\sum_i q_i[(y_i - y_{\rm b})\cos\phi - (x_i - x_{\rm b})\sin\phi]^2}{\sum_i q_i}$$

$$x_{\rm b} = \frac{\sum_i q_i x_i}{\sum_i q_i}, \quad y_{\rm b} = \frac{\sum_i q_i y_i}{\sum_i q_i}$$

where q_i is the charge in the pixel with coordinates (x_i, y_i). All pixels above a threshold of 2000 electrons in a $3.1 \times 3.1\,{\rm mm}^2$ box centered on $(x_{\rm b}, y_{\rm b})$ were included in the calculation. We did not perform a more refined analysis [13] that attempts to include only the pixels near the interaction point.

The results, shown in Fig. 5, demonstrate the polarization sensitivity of the detector. The data fit the expected functional form and peak around the independently measured polarization angle of the incident X-rays. All three data sets are consistent with the average modulation of 0.33 ± 0.03, which is also consistent with results from simulated data. The fit parameters are given in Table 1.

We have demonstrated a micropattern photoelectric polarimeter with a geometry suitable for the focal plane of an astronomical X-ray telescope. Amorphous silicon TFT anodes offer numerous possibilities for further improvement and extension. TFT arrays can be fabricated in large areas, opening the possibility of large-area collimated detectors, which might be a more practical alternative to an X-ray optic in a small satellite mission. Amorphous silicon can also be fabricated on a variety of optically thin substrates, including

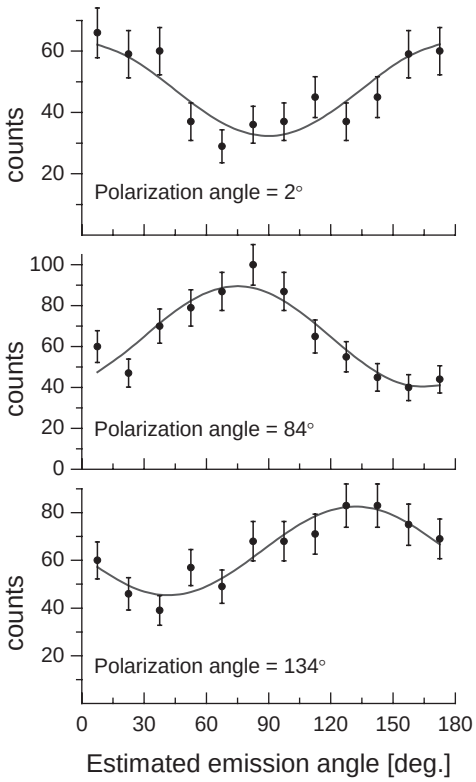

Fig. 5. Histograms of reconstructed emission angles for three polarization angles. The curves are fits to the data.

Table 1
Fit results to reconstructed emission angles

Polarization angle (°)	Fit parameters	
	μ	ϕ_{pol}
2	0.30 ± 0.06	0 ± 5
84	0.38 ± 0.05	75 ± 4
134	0.29 ± 0.05	132 ± 5

Stated errors are one standard deviation.

thin plastics [14]. Optically thin detectors would allow the stacking of multiple polarimeters at the focus of an X-ray mirror, with each layer optimized for a higher energy than the one before. In this way, the quantum efficiency and bandpass of the instrument could be even further extended.

Acknowledgements

This work was funded by NASA Grant no. NRA-01-01-HEA-021 and the GSFC Director's Discretionary Fund. Numerous individuals in the Laboratory for High Energy Astrophysics at GSFC supported this work. We particularly thank Mike Lenz, Bert Nahory, Norman Dobson, Drew Jones and Dr. Scott Owens for crucial technical support and Dr. Keith Jahoda for many helpful discussions. We also thank the members of the PARC process line for fabricating the TFT array.

References

[1] E. Costa, P. Soffitta, R. Bellazzini, A. Brez, N. Lumb, G. Spande, Nature 411 (2001) 662.
[2] R. Bellazzini, G. Spandre, N. Lumb, Nucl. Instr. and Meth. A 478 (2002) 13.
[3] R. Bellazzini, et al., IEEE Trans. Nucl. Sci. NS-49 (2002) 1216.
[4] R. Bellazzini, et al., Proc. SPIE 4843 (2003) 372.
[5] F. Sauli, Nucl. Instr. and Meth. A 386 (1997) 531.
[6] R.A. Street, in: R.A. Street (Ed.), Technology and Applications of Amorphous Silicon, Springer Series in Materials Science, Vol. 37, Springer, Berlin, 2000, p. 147.
[7] R. Petre, P.J. Serlemitsos, Space Sci. Rev. 40 (1985) 707.
[8] P.J. Serlemitsos, Y. Soong, Astrophys. Space Sci. 239 (1996) 177.
[9] J.K. Black, et al., Proc. SPIE 4140 (2000) 313.
[10] P. Deines-Jones, et al., Nucl. Instr. and Meth. A 478 (2002) 130.
[11] R. Street, et al., Proc. SPIE 3659 (1999) 36.
[12] R. Street, et al., Proc. SPIE 3977 (2000) 418.
[13] R. Bellazzini, et al., Proc. SPIE 4843 (2003) 383.
[14] D.B. Thomasson, et al. International Electron Devices Meeting Digest, 1998, p. 372.